

DOD-SA: Infrared-Visible Decoupled Object Detection with Single-Modality Annotations

Hang Jin¹, Chenqiang Gao^{1*}, Junjie Guo², Fangcen Liu², Kanghui Tian¹, Qinyao Chang³

¹ Sun Yat-sen University

² Chongqing University of Posts and Telecommunications

³ University of Electronic Science and Technology of China

Abstract

Infrared-visible object detection has shown great potential in real-world applications, enabling robust all-day perception by leveraging the complementary information of infrared and visible images. However, existing methods typically require dual-modality annotations to output detection results for both modalities during prediction, which incurs high annotation costs. To address this challenge, we propose a novel infrared-visible Decoupled Object Detection framework with Single-modality Annotations, called DOD-SA. The architecture of DOD-SA is built upon a Single-and Dual-Modality Collaborative Teacher-Student Network (CoSD-TSNet), which consists of a single-modality branch (SM-Branch) and a dual-modality decoupled branch (DMD-Branch). The teacher model generates pseudo-labels for the unlabeled modality, simultaneously supporting the training of the student model. The collaborative design enables cross-modality knowledge transfer from the labeled modality to the unlabeled modality, and facilitates effective SM-to-DMD branch supervision. To further improve the decoupling ability of the model and the pseudo-label quality, we introduce a Progressive and Self-Tuning Training Strategy (PaST) that trains the model in three stages: (1) pretraining SM-Branch, (2) guiding the learning of DMD-Branch by SM-Branch, and (3) refining DMD-Branch. In addition, we design a Pseudo Label Assigner (PLA) to align and pair labels across modalities, explicitly addressing modality misalignment during training. Extensive experiments on the DroneVehicle dataset demonstrate that our method outperforms state-of-the-art (SOTA).

Introduction

Infrared-visible (IR-VIS) object detection has attracted increasing attention in recent years due to its ability to leverage complementary spectral information for robust all-day perception (Zhang et al. 2021; Yuan, Wang, and Wei 2022; Ouyang et al. 2023a; Chen et al. 2024; Zhang et al. 2025). However, in practice, infrared and visible images are inevitably misaligned due to differences in imaging time or object motion (Zhu et al. 2023), even if they have been manually pre-registered through operations such as image cropping (Zeng et al. 2022) and affine transformation (Zhang and Ding 2022). This misalignment disrupts the feature learning

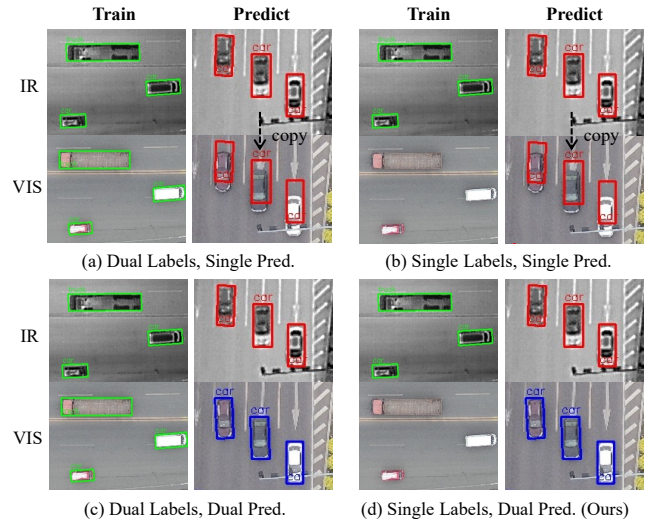


Figure 1: Comparison of multispectral object detection approaches. Green boxes: ground truth; red/blue boxes: predictions.

of the two modalities, thus affecting the detection performance of the model.

To address this issue, some approaches (Zhang et al. 2019b; Yuan, Wang, and Wei 2022; Yuan et al. 2024) utilized labels from both modalities to explicitly learn cross-modality offsets at the image or feature level, facilitating information fusion. Meanwhile, others (Yuan and Wei 2024; Ouyang, Jin, and Wang 2024; Chen et al. 2024; Guo et al. 2024b) enabled the model to implicitly learn such offsets by leveraging single-modality annotations. Nevertheless, these approaches share a single set of bounding box predictions across both modalities, as illustrated in Fig. 1(a) and (b).

In practical applications, object detection typically serves as a preliminary step for downstream processing. To ensure task reliability, many applications cannot depend solely on single-modality detection results. For example, when tracking targets in infrared and visible scenarios, reliance on only one modality's detections may cause tracking drift or target loss if the object is poorly localized or invisible in that modality. In such cases, incorporating complementary results from the other modality can effectively mitigate

*Corresponding author.

Copyright © 2026, Association for the Advancement of Artificial Intelligence (www.aaai.org). All rights reserved.

these failures. Therefore, outputting decoupled object positions for each modality is essential, particularly for multi-modal object tracking, behavioral analysis, and autonomous navigation of unmanned aerial vehicles (UAVs). Recently, DPDETR (Guo et al. 2024a) was proposed to address the decoupling problem. As shown in Fig. 1(c), this model can output positions of each object in both modalities during the prediction. However, this method requires annotations from both modalities, and the procedure of manually pairing boxes across modalities significantly increases annotation cost and complexity.

To this end, we propose a novel infrared-visible decoupled object detection framework with single-modality annotations (DOD-SA). As shown in Fig. 1(d), DOD-SA enables decoupled prediction while requiring labels from only one modality during training. Specifically, inspired by advances in semi-supervised object detection (Sohn et al. 2020; Liu et al. 2021; Xu et al. 2021; Zhou et al. 2021), we propose a Single- and Dual-Modality Collaborative Teacher-Student Network (CoSD-TSNet). The framework leverages the teacher model to generate pseudo-labels for unlabeled modality, addressing the issue of missing modality annotations. Further, a mutual learning mechanism between teacher and student enhances feature representation, while a single-modality detection branch (SM-Branch) is introduced to reinforce the training of the dual-modality decoupled branch (DMD-Branch), ensuring robust collaborative learning. To further improve the decoupling ability of the model and the quality of pseudo-labels, we propose a Progressive and Self-Tuning Training Strategy (PaST) which includes three training stages by first pretraining SM-Branch, then guiding the training of DMD-Branch by SM-Branch, and finally refining DMD-Branch through self-boosted learning. To filter and correct pseudo labels, we design a dedicated Pseudo Label Assigner (PLA). The PLA module employs shape-aware heuristics with a search region to match pseudo-labels from the unlabeled modality with ground truth from the labeled modality, while maintaining a dynamic pseudo-label bag that preserves high-quality label pairs across training epochs. This module explicitly addresses the modality misalignment issue due to the direct boxes location correcting, enabling the model to achieve better complementary representation learning. Extensive experiments on the DroneVehicle dataset (Sun et al. 2022) demonstrate that our method achieves SOTA performance, even outperforming fully supervised dual-modality SOTA methods while using only single-modality annotations. In summary, our contributions can be summarized as follows:

- To the best of our knowledge, We are the first to propose a novel framework, termed DOD-SA, which achieves accurate decoupled object detection on both infrared and visible modalities using single-modality annotations.
- We design a Single- and Dual-Modality Collaborative Teacher-Student Network (CoSD-TSNet) that leverages the teacher model to generate pseudo-labels for the unlabeled modality. This framework also enables the single-modality branch (SM-Branch) to guide the dual-modality decoupled detection branch (DMD-Branch) within a

unified Progressive and Self-Tuning Training Strategy (PaST), further improving the model’s decoupled detection performance.

- We introduce Pseudo Label Assigner (PLA) to match pseudo labels from unlabeled modality with ground truth from labeled modality and obtain high-quality label pairs, which also addresses modality misalignment explicitly.
- We validate DOD-SA on the DroneVehicle benchmark and show it achieves state-of-the-art performance with reduced annotation cost and superior robustness.

Related Work

Infrared-Visible Object Detection under Weak Misalignment Conditions

To address the modality misalignment issue, existing methods mainly focus on learning cross-modality offsets, which can be divided into two categories: dual-modality supervision and single-modality supervision, depending on whether both modalities are annotated.

Dual-Modality Supervision. AR-CNN (Zhang et al. 2019b) first tackled modality misalignment by explicitly learning geometric offsets using paired annotations, while TSFADet (Yuan, Wang, and Wei 2022) and CAGTDet (Yuan et al. 2024) improved alignment with considering scale/angle offset. DPDETR (Guo et al. 2024a) enabled decoupled predictions via modality-specific queries. However, these methods rely on costly paired annotations, limiting scalability in practice.

Single-Modality Supervision. C²former (Yuan and Wei 2024) computed attention between reference and sense modality features for fusion. DAMSDet (Guo et al. 2024b) introduced a deformable cross-attention module to extract fine-grained complementary information. OAFA (Chen et al. 2024) learnt offsets by separating common and private features. Zhang et al. (Zhang et al. 2025) proposed a Mean teacher-based box correction module to enhance representations. These methods use single-modality labels for supervision, but they only predict positions in one modality. Our approach enables dual-modality decoupled prediction with single-modality labels, creating a new practical setting.

Semi-Supervised Object Detection Method (SSOD)

SSOD methods aim to reduce annotation cost by utilizing unlabeled data, typically via consistency regularization or pseudo-labeling, when the latter is more widely adopted. STAC (Sohn et al. 2020) introduced a two-stage training paradigm. Unbiased Teacher (Liu et al. 2021) introduced focal loss (Lin et al. 2017) and the Exponential Moving Average (EMA) to address the class imbalance problem and improve pseudo labels quality. Soft Teacher (Xu et al. 2021) used the score of the pseudo-label as the weight of the loss. Efficient Teacher (Xu et al. 2023) divided the pseudo-labels into certain and uncertain labels. Despite significant advances, existing SSOD methods almost focus solely on single-modality object detection. In this paper, we apply teacher-student networks to dual-modality object detection to address the problem of single-modality annotations.

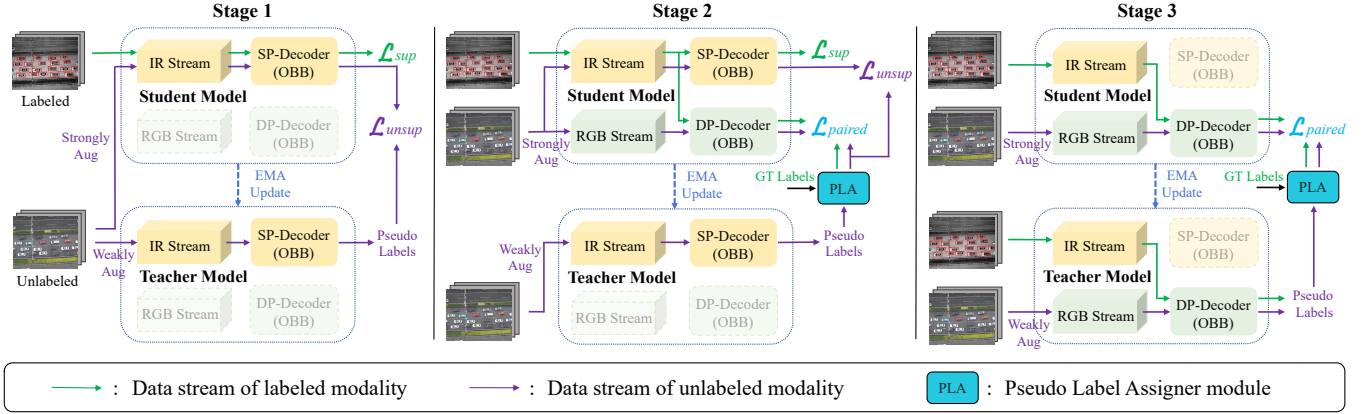


Figure 2: The overall framework of our proposed DOD-SA. It is based on a Single- and Dual-Modality Collaborative Teacher-Student Network, which effectively mines pseudo-labels for the unlabeled modality. The training process follows Progressive and Self-Tuning Training Strategy (PaST) consisting of three stages to continuously improve model performance. Furthermore, we design a Pseudo Label Assigner (PLA) to match the labeled-modality ground truth with the unlabeled-modality pseudo labels. After training, only the teacher’s DMD-Branch is retained. ‘OBB’ denotes oriented bounding box. The grayed-out parts indicate that they are excluded from the computation but remained in the model.

Label Assignment Strategy

Classical label assignment methods such as ATSS (Xie et al. 2021), PAA (Hong et al. 2020), AutoAssign (Yuan, Wang, and Wei 2022), OTA (Han et al. 2021), and TaskAlignedAssigner (Feng et al. 2021) have demonstrated strong performance under fully supervised settings. However, recent studies (Zhang et al. 2023; Wang et al. 2023) revealed that directly applying these strategies to semi-supervised object detection may lead to performance degradation, primarily due to the presence of noisy pseudo-labels and modality inconsistencies. In this paper, we propose a Pseudo Label Assigner (PLA) to enable application to dual-modality object detection under the single-modality annotations condition.

Method

Overall Architecture

As shown in Fig. 2, our DOD-SA is based on a Single- and Dual-Modality Collaborative Teacher-Student Network (CoSD-TSNet), designed to effectively address the issue of the missing modality annotations. The training process follows Progressive and Self-Tuning Training Strategy (PaST) consisting of three stages. In each stage, model’s specific branches are activated with different loss functions to further improve the quality of the pseudo labels. Moreover, we design a Pseudo Label Assigner (PLA) in the Stage 2 and 3 to generate decoupled label pairs. Additionally, our method is universally effective, regardless of whether the training set contains only visible or only infrared annotations. In this section, we consider the infrared modality as the labeled modality. Further details are introduced below.

Single- and Dual-Modality Collaborative Teacher-Student Network (CoSD-TSNet)

As presented in Fig. 2, CoSD-TSNet is a teacher-student framework, where the teacher/student model consists of two

parameter-unshared streams (IR Stream and RGB Stream), a single-modality decoder (SP-Decoder) and a dual-modality decoupled position decoder (DP-Decoder). Specifically, the IR/RGB Stream comprises a backbone, with the possible addition of an encoder, for feature extraction. The SP-Decoder contains a decoder and detection head, while the DP-Decoder further includes a feature fusion module before these components. For the decoding process, the SP-Decoder processes single-modality features, whereas the DP-Decoder integrates features from both modalities. Moreover, the branch that passes through SP-Decoder is called the single-modality branch (SM-Branch) and the branch that passes through DP-Decoder is called the dual-modality branch (DMD-Branch).

For the SM-Branch, it is similar to a single-modality detector, where it can only input an image from a single modality $x_m \in R^{H \times W \times 3}$, $m \in \{rgb, ir\}$ at a time and outputs one classification result \hat{c} and one modality’s position result \hat{b}_m , where $H \times W$ represents the spatial resolution. For the DMD-Branch, it functions as a decoupled position dual-modality detector, where it simultaneously processes images from two modalities $\{x_{ir}, x_{rgb}\}$ and outputs one classification result \hat{c} and decoupled position results for both modalities $\{\hat{b}_{ir}, \hat{b}_{rgb}\}$.

In our framework, the teacher model is responsible for mining pseudo-labels for unlabeled modality to address the issue of missing one modality annotations. Through the Exponential Moving Average (EMA) update mechanism, the results of the teacher are improved as the student is trained. We design this single- and dual-modality collaborative structure with the idea of using the single-modality detector to guide the training of the dual-modality detector. Additionally, it facilitates knowledge transfer from the labeled modality to the unlabeled modality by effectively leveraging the available labeled data.

Progressive and Self-Tuning Training Strategy (PaST)

To gradually mine high-quality pseudo-labels of the unlabeled modality and continuously improve model performance, we propose a Progressive and Self-Tuning Training Strategy (PaST). As illustrated in Fig. 2, PaST comprises three stages: (1) Stage 1. This stage aims to initially train the SM-Branch to develop preliminary capabilities for generating visible pseudo-labels. (2) Stage 2. The SM-Branch guides the training of the DMD-Branch to equip it with certain decoupled detection ability. (3) Stage 3. We optimize the entire DMD-Branch to refine detection results on the infrared and visible modality. Each stages is explained detailed below.

Stage 1. This stage only activates the SM-Branch and comprises two parts: burn-in and teacher-student mutual learning. The burn-in part aims to train the model on labeled data to establish initial detection capabilities for the labeled modality. During the teacher-student mutual learning part, knowledge is transferred from the labeled modality to the unlabeled modality, thereby enhancing the model’s detection performance on the unlabeled modality.

Burn-in: The labeled IR data x_{ir} are fed into the SM-Branch of the student model to obtain the IR predictions $\hat{y}_{ir}^s = \{\hat{c}, \hat{b}_{ir}\}$, which is supervised by IR ground truth $y_{ir} = \{c, b_{ir}\}$:

$$\mathcal{L}_{sup} = \mathcal{L}_{cls}(\hat{c}, c) + \mathcal{L}_{box}(\hat{b}_{ir}, b_{ir}), \quad (1)$$

\mathcal{L}_{cls} is classification loss and \mathcal{L}_{box} is rotated bounding box regression loss. This part continues for \mathcal{K}_1 epochs with the loss function \mathcal{L}_{sup} .

Teacher-Student Mutual Learning: The student model’s SM-Branch processes strongly augmented unlabeled RGB data x_{rgb}^* , while the teacher model’s SM-Branch receives a weakly augmented version x'_{rgb} of the same data. The teacher model outputs RGB pseudo labels $\tilde{y}_{rgb}^s = \{\tilde{c}, \tilde{b}_{rgb}\}$ and the student model outputs RGB predictions $\hat{y}_{rgb}^s = \{\hat{c}, \hat{b}_{rgb}\}$. To obtain more reliable and certain pseudo labels, we filter out pseudo labels below a batch-adaptive threshold which is explained in proposed Pseudo Label Assigner (PLA). Then, we use the filtered pseudo labels to supervise the RGB predictions of the student model:

$$\mathcal{L}_{unsup} = \mathcal{L}_{cls}(\hat{c}, \tilde{c}) + \mathcal{L}_{box}(\hat{b}_{rgb}, \tilde{b}_{rgb}). \quad (2)$$

This part continues \mathcal{K}_2 epochs with the loss function $\mathcal{L}_{sup} + \lambda \mathcal{L}_{unsup}$. Here, λ is an adaptive weight which linearly increases from 0 to 1.0 as training progresses.

Stage 2. We retain the activated modules of stage 1 and additionally activate the DMD-Branch in the student model where we copy the IR Stream parameters into the RGB Stream. The input x_{ir} and x_{rgb}^* are simultaneously input into the DMD-Branch of the student model, outputting the decoupled detection results $\hat{y}^d = \{\hat{c}, \hat{b}_{ir}, \hat{b}_{rgb}\}$. The input x'_{rgb} is fed into the SM-Branch of the teacher model, outputting RGB pseudo labels $\tilde{y}_{rgb}^s = \{\tilde{c}, \tilde{b}_{rgb}\}$. We propose PLA to match IR ground truth $y_{ir} = \{c, b_{ir}\}$ and RGB pseudo labels $\tilde{y}_{rgb}^s = \{\tilde{c}, \tilde{b}_{rgb}\}$ to form available supervised labels $y^d = \{c, b_{ir}, \tilde{b}_{rgb}\}$. This PLA will be introduced in detail

below. Subsequently, we use the matched labels to supervise the DMD-Branch:

$$\mathcal{L}_{paired} = \mathcal{L}_{cls}(\hat{c}, c) + \mathcal{L}_{boxir}(\hat{b}_{ir}, b_{ir}) + \mathcal{L}_{boxvis}(\hat{b}_{rgb}, \tilde{b}_{rgb}). \quad (3)$$

Additionally, we also adopt the \mathcal{L}_{sup} and \mathcal{L}_{unsup} mentioned in stage 1, except that \tilde{b}_{rgb} in \mathcal{L}_{unsup} is now the RGB results of PLA.

Stage 2 continues \mathcal{K}_3 epochs, the overall loss function of the stage is $\mathcal{L}_{sup} + \mathcal{L}_{unsup} + \mathcal{L}_{paired}$.

Stage 3. This stage only activates the DMD-Branch in the teacher and student model. The input x_{ir} and x'_{rgb} are simultaneously input into the DMD-Branch of the teacher model, outputting decoupled pseudo labels $\tilde{y}^d = \{\tilde{c}, \tilde{b}_{ir}, \tilde{b}_{rgb}\}$. Similarly, the student model outputs decoupled prediction results $\hat{y}^d = \{\hat{c}, \hat{b}_{ir}, \hat{b}_{rgb}\}$. We extract the RGB pseudo labels $\tilde{y}_{rgb} = \{\tilde{c}, \tilde{b}_{rgb}\}$ from \tilde{y}^d . These are then matched with the IR ground truth $y_{ir} = \{c, b_{ir}\}$ via PLA to generate supervision $y^d = \{c, b_{ir}, \tilde{b}_{rgb}\}$ for the student model. The loss function \mathcal{L}_{paired} is similar to Eq. (3), except that \tilde{b}_{rgb} is from DP-Decoder of the teacher model. This stage continues \mathcal{K}_4 epochs with the loss function \mathcal{L}_{paired} .

After the three-stage training of the model is completed, only the teacher network’s DMD-Branch structure is retained, ensuring robust and effective decoupled object detection on infrared and visible modalities.

Pseudo Label Assigner (PLA)

As presented in Fig. 3, our Pseudo Label Assigner (PLA) consists of three submodules: Pseudo Label Filter (PLF), Shape-aware Dual-modality Label Matcher (SDLM) and Dynamic Label Correction (DLC). These submodules are combined to provide DMD-Branch with dual-modality supervision information, through matching the infrared ground truth with visible pseudo-labels.

Pseudo Label Filter (PLF). We consider the classification probability of each RGB pseudo-label as the score:

$$score_i = \max_k p_{i,k}(\hat{c}), \quad (4)$$

where $p_{i,k}(\hat{c})$ denotes the probability of the i -th sample being classified as category k . Subsequently, similar to (Zhang et al. 2025), we use a batch-adaptive threshold to filter out low-quality samples, which is calculated as follows:

$$\tau = \mu - \sigma, \quad (5)$$

$$\mu = \frac{1}{N} \sum_{i=1}^N score_i, \quad (6)$$

$$\sigma = \sqrt{\frac{1}{N} \sum_{i=1}^N (score_i - \mu)^2}, \quad (7)$$

where τ , μ and σ represent the score threshold, the mean and the variance respectively, and N denotes the number of samples in a batch.

Shape-aware Dual-modality Label Matcher (SDLM). After filtering out high-quality RGB pseudo labels, we propose a Shape-aware Dual-modality Label Matcher (SDLM)

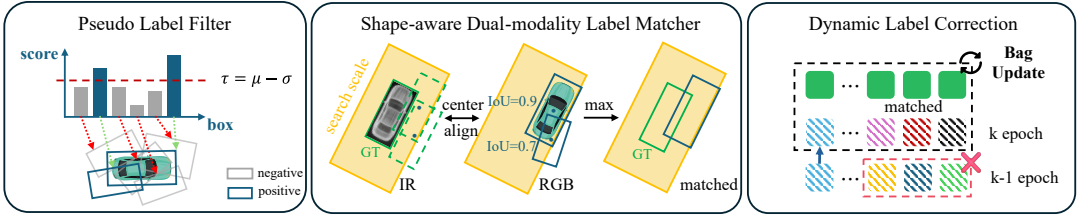


Figure 3: Pseudo Label Assigner. It consists of three components: (1) Pseudo Label Filter. It is used to filter out high-quality pseudo labels. (2) Shape-aware Dual-modality Label Matcher. It matches each infrared ground-truth bounding box with its corresponding visible pseudo label. (3) Dynamic Label Correction. We employ a dynamically updated label pairs bag to continuously correct the pseudo labels.

to pair the set of IR ground-truth bounding boxes $\{b_i^{\text{ir}}\}_{i=1}^N$ with the set of RGB pseudo labels $\{b_j^{\text{rgb}}\}_{j=1}^M$, where N and M represent their respective quantities, respectively. Each bounding box $b_i = (ct_{i,x}, ct_{i,y}, w_i, h_i, \theta_i)$ consists of the center coordinates $ct_i = (ct_{i,x}, ct_{i,y})$, width w_i , height h_i , and rotation angle θ_i . For each IR ground truth box b_i^{ir} , we define a search region:

$$\mathcal{S}_i = \left\{ (x, y) \mid (x, y) = (ct_{i,x}, ct_{i,y}) + R(\theta_i) \cdot \begin{bmatrix} \Delta x \\ \Delta y \end{bmatrix} \right\}, \quad (8)$$

$$(\Delta x, \Delta y) \in \left\{ \left(\pm \frac{\beta w_i}{2}, \pm \frac{\beta h_i}{2} \right) \right\}, \quad (9)$$

$$R(\theta_i) = \begin{bmatrix} \cos \theta_i & -\sin \theta_i \\ \sin \theta_i & \cos \theta_i \end{bmatrix}, \quad (10)$$

where $R(\theta_i)$ is a counterclockwise rotation matrix. β denotes a hyperparameter to adjust the aspect ratio of the search region. We use this search region to retain candidates with interior centers while excluding those already matched, obtaining the RGB candidate set C_i^{rgb} :

$$C_i^{\text{rgb}} = \left\{ b_j^{\text{rgb}} : ct_j \in \mathcal{S}_i \text{ and } b_j^{\text{rgb}} \notin P \right\}, \quad (11)$$

where P is the set of already paired boxes. We then compute the intersection over union (IoU) between each IR ground-truth box and all RGB boxes in C_i^{rgb} , then pair the IR box with the RGB candidate having the highest IoU. Since object shapes are nearly identical across modalities, the best-overlapping RGB pseudo-label likely corresponds to the same object.

$$b_j^* = \arg \max_{b_j^{\text{rgb}} \in C_i^{\text{rgb}}} \text{IoU} \left(b_i^{\text{ir}}, b_j^{\text{rgb}} \right), \quad (12)$$

where b_j^* denotes the successfully matched visible pseudo-label box.

Dynamic Label Correction (DLC). Considering relying solely on matched label pairs results in insufficient supervision, we incorporate the unmatched cases and maintain a dynamically updated label pairs bag to obtain more high-quality label pairs.

In the first epoch of Stage 2, we copy the unmatched infrared ground truth bounding boxes U_i^{ir} to the visible modality. These are then combined with the matched label pairs P_0 to initialize the dual-modality decoupled ground truth G_0 .

$$U_i^{\text{ir}} = \left\{ b_j^{\text{ir}} : b_j^{\text{ir}} \notin P_0 \right\}, \quad (13)$$

$$G_0 = P_0 \cup (U_i^{\text{ir}}, U_i^{\text{ir}}). \quad (14)$$

In the k -th epoch, let $(b_k^{\text{ir}}, b_k^{\text{rgb}})$ be one of the label pairs in G_k , where G_k denotes the dynamically updated infrared-visible label pairs bag in the k -th epoch. If in the next epoch, b_k^{ir} is successfully matched with a new RGB pseudo label $b_k^{\text{rgb}*}$, this label pair will be updated to $(b_k^{\text{ir}}, b_k^{\text{rgb}*})$. Otherwise, the label pair remains unchanged.

Experiments

Datasets and Evaluation Metrics

Dataset. We conduct experiments on the DroneVehicle Dataset (Sun et al. 2022), following the recent SOTA methods (Chen et al. 2024; Guo et al. 2024a; Shang et al. 2025; Zhang et al. 2024; Bao et al. 2025). This dataset is a large-scale object detection benchmark focused on drone-captured paired infrared and visible imagery. It contains 28,439 RGB-IR image pairs. Each modality has its own set of oriented bounding box annotations, covering five vehicle types: car, bus, truck, van, and freight car. To standardize the experimental protocol, we follow the methodology outlined in (Guo et al. 2024a) to process the annotations. After preprocessing, the dataset comprises 17,990 image pairs for training and 1,469 pairs for evaluation.

Evaluation metrics. We adopt the widely used mean Average Precision (mAP) at IoU threshold of 0.5 as the detection accuracy metric for the DroneVehicle dataset.

Implementation Details

We select DPDETR (Guo et al. 2024a) as our baseline model, which has excellent decoupled detection capability. Therefore, the IR and RGB Stream in our model is composed of a pre-trained ResNet50 (He et al. 2016) and an efficient encoder with feature map semantic level of $L=3$. The SP-Decoder follows the decoder of RTDETR (Zhao et al. 2024), and the DP-Decoder follows the decoder of DPDETR. Both decoder contain six layers, and we set the number of attention heads and selected queries to $H=8$ and $N=300$, respectively. For model training, we use AdamW optimizer with a weight decay of 1×10^{-4} . The initial learning rate is set to 1×10^{-7} and warm up to 1×10^{-4} by LinearWarmup and eventually reduced to 1×10^{-5} by PiecewiseDecay. The weak data augmentation includes random rotation, and flipping. Meanwhile, the strong augmentation

Model	Train image	Train label	Infrared-Test	Visible-Test
FSSD	IR	IR	72.72	-
YOLOX-X	IR	IR	73.24	-
Oriented RepPoints	IR	IR	68.00	-
RoITransformer	IR	IR	72.86	-
RTDETR(OBB)	IR	IR	77.93	-
FSSD	RGB	RGB	-	62.81
YOLOX-X	RGB	RGB	-	61.20
Oriented RepPoints	RGB	RGB	-	62.30
RoI Transformer	RGB	RGB	-	61.60
RTDETR(OBB)	RGB	RGB	-	72.92
AR-CNN (OBB)	IR+RGB	IR+RGB	71.58	-
TSFADet	IR+RGB	IR+RGB	73.06	-
C ² former	IR+RGB	IR+RGB	74.20	-
CAGTDet	IR+RGB	IR+RGB	74.57	-
DPDETR	IR+RGB	IR+RGB	79.90	79.81
Halfway Fusion(OBB)	IR+RGB	IR	68.19	-
CIAN(OBB)	IR+RGB	IR	70.23	-
MC-DETR	IR+RGB	IR	76.90	-
DDCINet	IR+RGB	IR	78.40	-
CCLDet	IR+RGB	IR	79.40	-
DOD-SA(Ours)	IR+RGB	IR	80.41	78.87
CALNet	IR+RGB	RGB	-	76.41
E2E-MFD	IR+RGB	RGB	-	77.40
M2FP	IR+RGB	RGB	-	78.70
DOD-SA(Ours)	IR+RGB	RGB	77.96	78.19

Table 1: Detection results (mAP, in %) on DroneVehicle Dataset. The best results are highlighted in **bold**. Infrared-Test denotes the test results of the trained model on the infrared images, while Visible-Test represents the test results on the visible images.

includes photometric transformations, spatial occlusions and blurring augmentation. The input size of our model is set to 640×640 and the batch size is 16. The EMA decay weight is 0.9999. The training epochs are set as: $\mathcal{K}_1 = 20$, $\mathcal{K}_2 = 10$, $\mathcal{K}_3 = 15$ and $\mathcal{K}_4 = 20$. The hyperparameter β in Pseudo Label Assigner is set to 1.0. We conduct experiments on an Nvidia RTX A6000 GPU.

Comparisons with state-of-the-art

We compare our proposed DOD-SA with five state-of-the-art single modality detectors, including FSSD (Li, Yang, and Zhou 2017), YOLOX-X (Ge et al. 2021), Oriented RepPoints (Li et al. 2022), RoI Transformer (Ding et al. 2019) and RTDETR (Zhao et al. 2024). We also make a comparison with thirteen multispectral object detection methods, including AR-CNN (Zhang et al. 2021), TSFADet (Yuan, Wang, and Wei 2022), C²former (Yuan and Wei 2024), CAGTDet (Yuan et al. 2024), DPDETR (Guo et al. 2024a), Halfway Fusion (Wagner et al. 2016), CIAN (Zhang et al. 2019a), MC-DETR (Ouyang et al. 2023b), DDCINet (Bao et al. 2025), CCLDet (Shang et al. 2025), CALNet (He et al. 2023), E2E-MFD (Zhang et al. 2024) and M2FP (Ouyang, Jin, and Wang 2024).

Quantitative comparison. As shown in Tab. 1, DOD-SA outperforms single-modality methods under the same training label conditions. Compared to dual-modality networks, it achieves state-of-the-art performance (80.41% in IR, 78.87% in RGB) when trained only on IR labels, surpassing CLDet by 1% mAP in infrared testing. Even when trained on RGB labels, our method delivers strong decoupled results (77.96% in IR, 78.19% in RGB), demon-

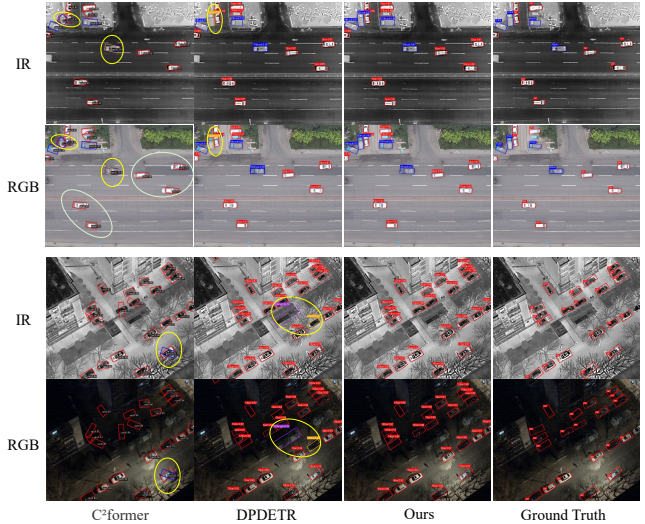


Figure 4: Representative results of different methods on the DroneVehicle dataset: daytime scenarios (top) vs nighttime scenarios (bottom). Yellow circles denote false positives and light green circles show localization errors (decoupling failures).

ing effective modality-generalization. Additionally, our approach outperforms DPDETR and other dual-annotation methods, as the teacher-student architecture acts as a consistency regularizer, enriching learned representations.

Qualitative comparison. Fig. 4 shows some representative detection results of different methods, which can be observed that C²Former produces results for only one modality, leading to large positional errors in the other modality. In contrast, our DOD-SA accurately predicts decoupled object positions in both infrared and visible modalities, even in dark or highly misaligned scenarios. Our method matches or outperforms DPDETR, which occasionally makes prediction errors. This is because DOD-SA effectively generates pseudo-labels and leverages complementary features, achieving strong performance in both modalities.

Ablation Studies

Effect of PaST. As shown in Tab. 2, we analyze the necessity of each stage in PaST by ablating different training stages (50 epochs each). Comparing ours and Exp. IV shows Stage 1 improves mAP by 0.67%, as it helps the single-modality detector develop initial pseudo-label mining capability, ensuring better guidance for Stage 2. Exp. III vs. Exp. IV verifies the importance of SM-Branch in guiding the training of DMD-Branch in Stage 2. Finally, Exp. V vs. ours shows that Stage 3 boosts mAP by 0.86% through teacher-student mutual learning, further refining the DMD-Branch.

Effect of PLF. We evaluate the impact of varying the threshold value τ in the Pseudo Label Filter (PLF). As shown in Table 3, the model performance degrades significantly without pseudo-label filtering (w/o PLF). The mAP varies with different thresholds, showing that a fixed τ cannot balance pseudo-label quantity and quality. Dynamically

	Stage 1	Stage 2	Stage 3	IR	RGB
I	✓			75.75	48.70
II		✓		79.44	77.68
III			✓	79.19	65.59
IV		✓	✓	79.74	78.18
V	✓	✓	✓	79.55	77.77
Ours	✓	✓	✓	80.41	78.87

Table 2: Ablation study of PaST.

Table 3: Ablation study of PLF.

	Method	IR	RGB
I	w/o PLF	78.99	77.85
II	$\tau=0.4$	79.01	77.72
III	$\tau=0.6$	79.51	78.47
IV	$\tau=0.8$	79.21	78.24
Ours	PLF	80.41	78.87

Table 4: Ablation study of SDLM.

	Method	IR	RGB
I	w/o DLC	79.18	77.78
II	w/o DU	79.27	78.57
III	CBC	79.65	78.12
Ours	DLC	80.41	78.87

Table 5: Ablation study of DLC.

adjusting τ through distribution adaptation yields the best results, demonstrating PLF’s importance for model training.

Effect of SDLM. To validate the effectiveness of our Shape-aware Dual-modality Label Matcher (SDLM), we conduct several comparative experiments. The IoU Match Strategy uses a label-pairing method similar to that applied to the DroneVehicle dataset. Results are shown in Tab. 4. Using ground-truth labels from the labeled modality as pseudo-labels (w/o DLM) improves mAP by 0.64% compared to not using pseudo-labels at all. Our baseline, the IoU Match Strategy, increases mAP to 79.55% by addressing label assignment. When we apply DLM for label matching, mAP further improves by 0.86% on IR and 1.35% on RGB. These results confirm the effectiveness of our approach.

Effect of DLC. We perform an ablation study to evaluate the impact of Dynamic Label Correction (DLC). As shown in Table 5, using only matched label pairs (w/o DLC) results in 79.18% mAP on IR. Including unmatched labels (w/o DU) improves performance, highlighting their importance. Cross-modality BBox Correction (CBC) (Zhang et al. 2025) uses a progressive center correction strategy to adjust shifted ground-truth boxes in the unlabeled modality, which may introduce label ambiguity because the smoothed labels can be misplaced, thus misleading the model during training. In contrast, our method dynamically updates the label bag to mitigate this issue, yielding performance improvements of 0.76% on IR and 0.75% on RGB compared to CBC.

Visualization of Pseudo Labels. To illustrate the effectiveness of pseudo-labels correction from unlabeled modality, we visualize the pseudo-labels mined by our model. Fig. 5 (a) and (b) illustrate that our model can correct the offsets caused by high-speed motion of objects. Fig. 5 (c) shows that even when the object is stationary, misalignment can occur due to the shooting angle and the drone motion. Nevertheless, our method effectively corrects this issue. Fig. 5 (d), (e) and (f) demonstrate that our approach remains effective in difficult conditions like low light or occlusion.

Robustness to Position Shift

To evaluate the robustness of our method against modality misalignment problem, we introduce positional offsets to test images set. We keep the IR images fixed while applying spatial offsets along both the x-axis and y-axis to the RGB images. The pixel value variations are defined within the range $\{(\Delta x, \Delta y) \mid \Delta x, \Delta y \in [15, -15]; \Delta x, \Delta y \in \mathbb{Z}\}$. As shown in Fig. 6, the performance of our method on the IR test set is more stable under these shifts compared to the baseline. For the RGB test set, both models perform similarly, but our method is slightly more stable under small shifts. This indicates that our method enhances the model’s

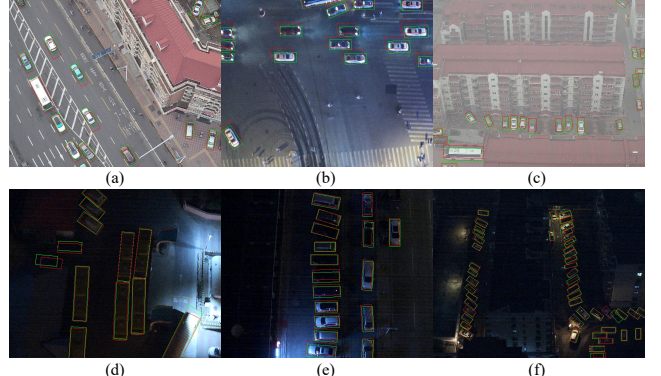


Figure 5: Visualization of pseudo labels on DroneVehicle. Red boxes represent the IR ground truth copied from the infrared image to the visible image, while green boxes represent the corrected RGB pseudo labels.

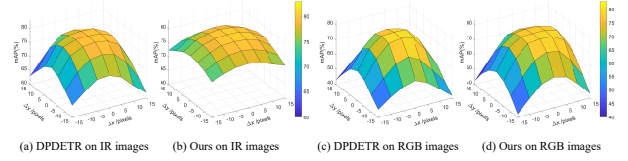


Figure 6: Performance comparison under various positional shifts.

understanding of the correspondences between each pair of objects across the two modalities and makes it more robust to positional misalignment.

Conclusion

In this paper, we propose DOD-SA, a novel infrared-visible decoupled object detection framework with single-modality annotations. Our Collaborative Single- and Dual-Modality Teacher-Student Network (CoSD-TSNet) leverages the single-modality branch (SM-Branch) to enhance the training of the dual-modality decoupled branch (DMD-Branch) via a Progressive and Self-Tuning Training Strategy (PaST), which further improve the performance of the model. Additionally, we introduce a Pseudo Label Assigner (PLA) to match the ground-truth from labeled modality with mined pseudo-labels from the unlabeled modality. Experiments on the DroneVehicle dataset demonstrate the superiority of DOD-SA over state-of-the-art methods. Ablation studies validate the necessity of each component, and our approach exhibits strong robustness to positional shifts.

References

Bao, W.; Huang, M.; Hu, J.; and Xiang, X. 2025. Dual dynamic cross-modal interaction network for multimodal remote sensing object detection. *IEEE Transactions on Geoscience and Remote Sensing*.

Chen, C.; Qi, J.; Liu, X.; Bin, K.; Fu, R.; Hu, X.; and Zhong, P. 2024. Weakly misalignment-free adaptive feature alignment for uav-based multimodal object detection. In *Proceedings of the IEEE/CVF Conference on Computer Vision and Pattern Recognition*, 26836–26845.

Ding, J.; Xue, N.; Long, Y.; Xia, G.-S.; and Lu, Q. 2019. Learning ROI transformer for oriented object detection in aerial images. In *Proceedings of the IEEE/CVF conference on computer vision and pattern recognition*, 2849–2858.

Feng, C.; Zhong, Y.; Gao, Y.; Scott, M. R.; and Huang, W. 2021. Tood: Task-aligned one-stage object detection. In *2021 IEEE/CVF International Conference on Computer Vision (ICCV)*, 3490–3499. IEEE Computer Society.

Ge, Z.; Liu, S.; Wang, F.; Li, Z.; and Sun, J. 2021. Yolox: Exceeding yolo series in 2021. *arXiv preprint arXiv:2107.08430*.

Guo, J.; Gao, C.; Liu, F.; and Meng, D. 2024a. DPDETR: Decoupled position detection transformer for infrared-visible object detection. *arXiv preprint arXiv:2408.06123*.

Guo, J.; Gao, C.; Liu, F.; Meng, D.; and Gao, X. 2024b. Damsdet: Dynamic adaptive multispectral detection transformer with competitive query selection and adaptive feature fusion. In *European Conference on Computer Vision*, 464–481. Springer.

Han, J.; Ding, J.; Li, J.; and Xia, G.-S. 2021. Align deep features for oriented object detection. *IEEE transactions on geoscience and remote sensing*, 60: 1–11.

He, K.; Zhang, X.; Ren, S.; and Sun, J. 2016. Deep residual learning for image recognition. In *Proceedings of the IEEE conference on computer vision and pattern recognition*, 770–778.

He, X.; Tang, C.; Zou, X.; and Zhang, W. 2023. Multispectral object detection via cross-modal conflict-aware learning. In *Proceedings of the 31st ACM International Conference on Multimedia*, 1465–1474.

Hong, D.; Chanussot, J.; Yokoya, N.; Kang, J.; and Zhu, X. X. 2020. Learning-shared cross-modality representation using multispectral-LiDAR and hyperspectral data. *IEEE Geoscience and Remote Sensing Letters*, 17(8): 1470–1474.

Li, W.; Chen, Y.; Hu, K.; and Zhu, J. 2022. Oriented repoints for aerial object detection. In *Proceedings of the IEEE/CVF conference on computer vision and pattern recognition*, 1829–1838.

Li, Z.; Yang, L.; and Zhou, F. 2017. FSSD: feature fusion single shot multibox detector. *arXiv preprint arXiv:1712.00960*.

Lin, T.-Y.; Goyal, P.; Girshick, R.; He, K.; and Dollár, P. 2017. Focal loss for dense object detection. In *Proceedings of the IEEE international conference on computer vision*, 2980–2988.

Liu, Y.-C.; Ma, C.-Y.; He, Z.; Kuo, C.-W.; Chen, K.; Zhang, P.; Wu, B.; Kira, Z.; and Vajda, P. 2021. Unbiased teacher for semi-supervised object detection. *arXiv preprint arXiv:2102.09480*.

Ouyang, J.; Jin, P.; and Wang, Q. 2024. Multimodal feature-guided pre-training for RGB-T perception. *IEEE Journal of Selected Topics in Applied Earth Observations and Remote Sensing*.

Ouyang, J.; Wang, Q.; Liu, J.; Qu, X.; Song, J.; and Shen, T. 2023a. Multi-modal and cross-scale feature fusion network for vehicle detection with transformers. In *2023 International Conference on Machine Vision, Image Processing and Imaging Technology (MViPIT)*, 175–180. IEEE.

Ouyang, J.; Wang, Q.; Liu, J.; Qu, X.; Song, J.; and Shen, T. 2023b. Multi-modal and cross-scale feature fusion network for vehicle detection with transformers. In *2023 International Conference on Machine Vision, Image Processing and Imaging Technology (MViPIT)*, 175–180. IEEE.

Shang, X.; Li, N.; Li, D.; Lv, J.; Zhao, W.; Zhang, R.; and Xu, J. 2025. Ccldet: A cross-modality and cross-domain low-light detector. *IEEE Transactions on Intelligent Transportation Systems*.

Sohn, K.; Zhang, Z.; Li, C.-L.; Zhang, H.; Lee, C.-Y.; and Pfister, T. 2020. A simple semi-supervised learning framework for object detection. *arXiv preprint arXiv:2005.04757*.

Sun, Y.; Cao, B.; Zhu, P.; and Hu, Q. 2022. Drone-based RGB-infrared cross-modality vehicle detection via uncertainty-aware learning. *IEEE Transactions on Circuits and Systems for Video Technology*, 32(10): 6700–6713.

Wagner, J.; Fischer, V.; Herman, M.; Behnke, S.; et al. 2016. Multispectral Pedestrian Detection using Deep Fusion Convolutional Neural Networks. In *ESANN*, volume 587, 509–514.

Wang, X.; Yang, X.; Zhang, S.; Li, Y.; Feng, L.; Fang, S.; Lyu, C.; Chen, K.; and Zhang, W. 2023. Consistent-teacher: Towards reducing inconsistent pseudo-targets in semi-supervised object detection. In *Proceedings of the IEEE/CVF conference on computer vision and pattern recognition*, 3240–3249.

Xie, X.; Cheng, G.; Wang, J.; Yao, X.; and Han, J. 2021. Oriented R-CNN for object detection. In *Proceedings of the IEEE/CVF international conference on computer vision*, 3520–3529.

Xu, B.; Chen, M.; Guan, W.; and Hu, L. 2023. Efficient teacher: Semi-supervised object detection for yolov5. *arXiv preprint arXiv:2302.07577*.

Xu, M.; Zhang, Z.; Hu, H.; Wang, J.; Wang, L.; Wei, F.; Bai, X.; and Liu, Z. 2021. End-to-end semi-supervised object detection with soft teacher. In *Proceedings of the IEEE/CVF international conference on computer vision*, 3060–3069.

Yuan, M.; Shi, X.; Wang, N.; Wang, Y.; and Wei, X. 2024. Improving RGB-infrared object detection with cascade alignment-guided transformer. *Information Fusion*, 105: 102246.

Yuan, M.; Wang, Y.; and Wei, X. 2022. Translation, scale and rotation: cross-modal alignment meets RGB-infrared

vehicle detection. In *European Conference on Computer Vision*, 509–525. Springer.

Yuan, M.; and Wei, X. 2024. C 2 former: Calibrated and complementary transformer for rgb-infrared object detection. *IEEE Transactions on Geoscience and Remote Sensing*.

Zeng, H.; Li, L.; Cao, Z.; and Zhang, L. 2022. Grid Anchor Based Image Cropping: A New Benchmark and An Efficient Model. *IEEE Transactions on Pattern Analysis and Machine Intelligence*, 1304–1319.

Zhang, J.; Cao, M.; Xie, W.; Lei, J.; Li, D.; Huang, W.; Li, Y.; and Yang, X. 2024. E2e-mfd: Towards end-to-end synchronous multimodal fusion detection. *Advances in Neural Information Processing Systems*, 37: 52296–52322.

Zhang, L.; Liu, Z.; Zhang, S.; Yang, X.; Qiao, H.; Huang, K.; and Hussain, A. 2019a. Cross-modality interactive attention network for multispectral pedestrian detection. *Information Fusion*, 50: 20–29.

Zhang, L.; Liu, Z.; Zhu, X.; Song, Z.; Yang, X.; Lei, Z.; and Qiao, H. 2021. Weakly aligned feature fusion for multimodal object detection. *IEEE Transactions on Neural Networks and Learning Systems*.

Zhang, L.; Zhu, X.; Chen, X.; Yang, X.; Lei, Z.; and Liu, Z. 2019b. Weakly aligned cross-modal learning for multispectral pedestrian detection. In *Proceedings of the IEEE/CVF international conference on computer vision*, 5127–5137.

Zhang, R.; Xu, C.; Xu, F.; Yang, W.; He, G.; Yu, H.; and Xia, G.-S. 2023. Rethinking scale imbalance in semi-supervised object detection for aerial images. *arXiv preprint arXiv:2310.14718*.

Zhang, Y.; Yang, W.; Xu, C.; Hu, Q.; Xu, F.; and Xia, G.-S. 2025. Mitigating the Impact of Prominent Position Shift in Drone-based RGBT Object Detection. *arXiv preprint arXiv:2502.09311*.

Zhang, Z.; and Ding, Y. 2022. Adaptive Affine Transformation: A Simple and Effective Operation for Spatial Misaligned Image Generation. In *Proceedings of the 30th ACM International Conference on Multimedia*.

Zhao, Y.; Lv, W.; Xu, S.; Wei, J.; Wang, G.; Dang, Q.; Liu, Y.; and Chen, J. 2024. Detrs beat yolos on real-time object detection. In *Proceedings of the IEEE/CVF conference on computer vision and pattern recognition*, 16965–16974.

Zhou, Q.; Yu, C.; Wang, Z.; Qian, Q.; and Li, H. 2021. Instant-teaching: An end-to-end semi-supervised object detection framework. In *Proceedings of the IEEE/CVF conference on computer vision and pattern recognition*, 4081–4090.

Zhu, Y.; Sun, X.; Wang, M.; and Huang, H. 2023. Multi-modal feature pyramid transformer for rgb-infrared object detection. *IEEE Transactions on Intelligent Transportation Systems*, 24(9): 9984–9995.